Journal of Inorganic Biochemistry 244 (2023) 112222

Contents lists available at ScienceDirect

Journal of Inorganic Biochemistry

journal homepage: www.elsevier.com/locate/jinorgbio

Elucidating the concentration-dependent effects of thiocyanate binding to carbonic anhydrase☆

José Malanho Silva [a,b], Linda Cerofolini [a,c], Ana Luísa Carvalho [b,d], Enrico Ravera [a,c,e], Marco Fragai [a,c,e], Giacomo Parigi [a,c,e], Anjos L. Macedo [b,d], Carlos F.G.C. Geraldes [f,g], Claudio Luchinat [a,c,e,h,*]

[a] Magnetic Resonance Center (CERM), University of Florence, Sesto Fiorentino 50019, Italy
[b] UCIBIO, Department of Chemistry, NOVA School of Science and Technology, Universidade NOVA de Lisboa, 2819-516 Caparica, Portugal
[c] Department of Chemistry "Ugo Schiff", University of Florence, Sesto Fiorentino 50019, Italy
[d] Associate Laboratory i4HB – Institute for Health and Bioeconomy, NOVA School of Science and Technology, Universidade NOVA de Lisboa, Caparica, Portugal
[e] Consorzio Interuniversitario Risonanze Magnetiche Metallo Proteine (CIRMMP), Sesto Fiorentino, 50019, Italy
[f] Department of Life Sciences, Faculty of Science and Technology, 3000-393 Coimbra, Portugal
[g] Coimbra Chemistry Center- Institute of Molecular Sciences (CCC-IMS), University of Coimbra, 3004-535 Coimbra, Portugal
[h] Giotto Biotech, S.R.L, Sesto Fiorentino, Florence 50019, Italy

ARTICLE INFO

Keywords:
Human carbonic anhydrase II
NMR
EPR
Sodium thiocyanate
Paramagnetism
Structural biology

ABSTRACT

Many proteins naturally carry metal centers, with a large share of them being in the active sites of several enzymes. Paramagnetic effects are a powerful source of structural information and, therefore, if the native metal is paramagnetic, or it can be functionally substituted with a paramagnetic one, paramagnetic effects can be used to study the metal sites, as well as the overall structure of the protein. One notable example is cobalt(II) substitution for zinc(II) in carbonic anhydrase. In this manuscript we investigate the effects of sodium thiocyanate on the chemical environment of the metal ion of the human carbonic anhydrase II. The electron paramagnetic resonance (EPR) titration of the cobalt(II) protein with thiocyanate shows that the EPR spectrum changes from A-type to C-type on passing from 1:1 to 1:1000-fold ligand excess. This indicates the occurrence of a change in the electronic structure, which may reflect a sizable change in the metal coordination environment in turn caused by a modification of the frozen solvent glass. However, paramagnetic nuclear magnetic resonance (NMR) data indicate that the metal coordination cage remains unperturbed even in 1:1000-fold ligand excess. This result proves that the C-type EPR spectrum observed at large ligand concentration should be ascribed to the low temperature at which EPR measurements are performed, which impacts on the structure of the protein when it is destabilized by a high concentration of a chaotropic agent.

1. Introduction

Carbonic anhydrases (CAs) are zinc(II) metalloenzymes [1] present in almost all living organisms. In mammals, the enzyme is present in several isoforms and, among the 15 isoforms of human carbonic anhydrases (hCA), the most abundant is the second isoform, which is mostly present in blood [2]. CAs catalyze the interconversion between carbon dioxide and hydrogencarbonate. Furthermore, hCA has esterase activity towards esters of carboxylic, sulfonic and phosphoric acid derivatives [3].

The zinc(II) ion present in the active center of hCAII is coordinated by four ligands, His94 and His96 through the Nε2 atoms, His 119 through Nδ1, and a hydroxide ion or a water molecule, depending on pH [4]. The zinc(II) ion can be replaced by a variety of metal ions, such as paramagnetic cobalt(II), nickel(II) and copper(II). It has been shown that if zinc(II) is substituted with cobalt(II), the enzyme maintains a

☆ Dedicated to F. Ann Walker, an excellent scientist and a very dear friend to many of us. Since the early times of the NMR of paramagnetic molecules in the seventies, Ann shared with us the enthusiasm and the drive to understand all the intricacies of the electron-nucleus interactions. We had in common with Ann a strong interest in the behavior of paramagnetic hemes, which later evolved into the more challenging interest in heme proteins and in their structure-function relationships.

* Corresponding author at: Magnetic Resonance Center (CERM), University of Florence, Sesto Fiorentino 50019, Italy.
E-mail address: luchinat@cerm.unifi.it (C. Luchinat).

https://doi.org/10.1016/j.jinorgbio.2023.112222
Received 14 February 2023; Received in revised form 28 March 2023; Accepted 9 April 2023
Available online 11 April 2023

good fraction of its enzymatic activity [5–7], whereas manganese(II), iron(II), copper(II), and nickel(II) hCAII derivatives are inactive [6]. The coordination geometries of the metal-substituted enzymes are different from that of zinc [5,8,9], except for cobalt(II), which remains essentially tetra-coordinated in its active form [5,10–13].

Paramagnetic carbonic anhydrase derivatives have been studied throughout several decades, and even recently they have being used to solve questions regarding the origin of paramagnetic NMR shifts [14]. In particular, the electronic and magnetic properties of high-spin cobalt(II) make it a powerful UV–vis, NMR and EPR spectroscopic probe in biological systems.

Cobalt(II) has a d^7 electronic configuration and, when bound to proteins, it commonly adopts a high-spin configuration, with an electronic spin $S = 3/2$ (see Fig. 1). The low symmetry environment of cobalt (II) in proteins removes the orbital degeneracy, making the excited states relatively close in energy to the ground state. This proximity in energy causes the Orbach electron spin relaxation mechanism to be very efficient so that, depending on the geometry of the metal coordination, the electron spin relaxation times typically ranges between 1 and 10 ps [15]. This very fast electron relaxation prevents the acquisition of EPR spectra at room temperature. Only around liquid helium temperature electron relaxation is slowed down enough to allow for the acquisition of EPR spectra. Fast electron relaxation, however, provides a rather inefficient mechanism for paramagnetic nuclear spin relaxation, thus the NMR resonances are not severely broadened. The vicinity of the excited states to the ground state is also responsible for large magnetic susceptibility anisotropies ($\Delta\chi$) [16], which cause large pseudocontact shifts (PCSs) and paramagnetic residual dipolar couplings (RDCs). PCSs and paramagnetic RDCs are long range structural restraints extensively used for the structural characterization of paramagnetic proteins [17–26]. The information content in terms of molecular and electronic structures of paramagnetic NMR shifts and EPR spectra were deeply investigated by F. Ann Walker [27–30], who provided outstanding contributions especially for the characterization of heme proteins and iron complexes.

The binding of inhibitors can change the coordination enviroment of the metal ion. 2D NMR studies of cobalt(II)-CAs adducts started in the 1980's, with the investigation of the ClO_4^-, NO_3^- and NCS^- ligands in solution [31,32]; these studies continued with the recent works on the oxalate and furosemide adducts of cobalt(II)-hCAII at different pH values [16], and the solid-state NMR studies of the furosemide and sulpiride adducts [33]. The presence of inhibitors can lead to pseudo-tetrahedral coordination, square-pyramidal coordination, or to an equilibrium between the two. Information on the coordination geometry can be obtained from ligand field d-d transitions studies: inhibitors like SCN^-, I^-, formate, acetate, oxalate, nitrate and 1,2,3-triazole ($\varepsilon_{max} < 200\ M^{-1}\ cm^{-1}$) give rise to five-coordinate species; sulfonamides, NCO^-, CN^-, aniline, imidazole (high pH), and 1,2,4-triazole ($\varepsilon_{max} > 300\ M^{-1}\ cm^{-1}$) give rise to pseudo-tetrahedral species; and HCO_3^-, N_3^-, F^-, Cl^-, Br^-, phosphate, benzoate and imidazole (low pH) ($\varepsilon_{max} = 200–300\ M^{-1}\ cm^{-1}$) lead to four-to-five coordinate equilibria [7].

Also the shape of the EPR spectrum (leading to type A, B, or C classification) has been related to the cobalt coordination number [34]: type A spectra (obtained by binding of acetate, nitrate, thiocyanate, azide or iodide) have two transitions with g values around 6.1–6.8 and 2.3–2.9 and in some cases a third transition around 1.6–1.8; type B spectra (observed by binding of acetazolamide, sulfonamides, cyanate or cyanide) show a sharp feature in the low-field region of the spectrum with g values around 5.8–6.2, 2.2–2.8, and 1.5–1.8; and type C spectra, with a single quasi symmetrical line centered at g values around 3.8–4.0, arise from an excess of ligands like iodide, thiocyanate and imidazole, that may be able to bind in a secondary site inside the active site pocket, thus further modifying the spectral features [34].

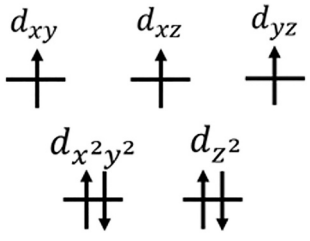

Fig. 1. Electronic configuration of high-spin cobalt(II) in idealized tetrahedral geometry.

The NMR studies have shown that type A and type B ligands have very different magnetic susceptibility anisotropies ($\Delta\chi$) [16,31,32]. Type A ligands produce $\Delta\chi$ values that are at least twice in absolute value of those of type B ligands, with correspondingly larger PCSs. So far, there are no NMR studies of type C ligands.

The aim of this work is to investigate the effects caused by thiocyanate binding to cobalt(II)-hCAII depending on its concentration. In fact, thiocyanate generates a type A EPR spectrum when added in stoichiometric amounts to cobalt(II)-CA, and a type C spectrum when added in large excess [34]. The evaluation of the magnetic susceptibility anisotropy of cobalt(II)-hCAII in the presence of increasing amounts of thiocyanate may provide information on the origin of the different EPR spectra. In this study, a double mutant of hCAII (DM-hCAII) [14] was used to avoid the binding of metal ions to a secondary site [35].

2. Materials and methods

2.1. Double mutant construct

The wild-type form of hCAII was mutated in two positions, H3N and H4N, to avoid the binding of transition metals in the secondary site [9,14,35]. The hCAII double mutant was cloned following a standard PCR protocol.

2.2. Expression and purification of DM-hCAII

The expression and purification of DM-hCAII, based on the published protocol [33], was optimized as indicated. The expression vector, pCAM coding the DM-hCAII, was inserted in competent *Escherichia coli* BL21 (DE3) using a standard heat shock protocol. The culture was in LB-Agar supplemented with 1% glucose and ampicillin. The plates were incubated at 37 °C overnight. The following day a successful transformant colony was selected and resuspended in 500 μL of sterile water. 50 μL of culture were plated into 2 plates of LB-Agar supplemented with 1% glucose and ampicillin.

The plates were incubated overnight at 37 °C. The following day, the cells were scraped from one plate to 1 L of LB media supplemented with 1% glucose and ampicillin. The absorbance at 600 nm was measured until 0.6 OD, and then the LB cultures were centrifuged at 4000 rpm for 15 min. The pellet was resuspended in M9 media, supplemented with $MgSO_4$, $CaCl_2$, 0.5 mM $ZnSO_4$, 1.2 g/L of ^{15}N-enriched $(NH_4)_2SO_4$, 3 g/L glucose and ampicillin. The culture was incubated at 37 °C, 160 rpm for 30 min. Afterwards, 1 mM IPTG was added, and the temperature decreased to 25 °C. The culture was incubated overnight. The protein expression was halted by centrifuging the cultures at 7500 rpm for 20 min. The harvested cell pellet was stored at −20 °C.

The cell pellet was resuspended in a final volume of 70 mL of 20 mM Tris-SO_4 buffer, 0.5 mM $ZnSO_4$, pH 8. The cells were sonicated for 30 s with a resting period on ice for 3 min, and this was repeated for a total of 10 times. The lysate was ultracentrifuged at 40000 rpm for 40 min and the supernatant was filtered with a 0.45 micra filter.

The lysate was firstly purified in a 5 mL Histrap FF, using an AKTA Prime System, previously equilibrated with 20 mM Tris-SO_4, 0.5 mM $ZnSO_4$ pH 8. The protein was eluted with a gradient of 20 column volumes from 0 to 50% buffer containing 20 mM Tris-SO_4, 500 mM imidazole, 0.5 mM $ZnSO_4$ pH 8. The eluted fractions were analyzed by SDS-PAGE, and the fractions containing hCAII were pooled. Pooled fractions

were concentrated using a 10,000 MWCO Amicon centrifugation device to 10 mL.

As a second purification step a 320 mL Superdex 75 pg 26/60 size exclusion column was used in an AKTA Prime system, with a running buffer of 50 mM Sodium Phosphate pH 7, at 2.5 mL/min. The purified protein was pooled and stored at 4 °C.

2.3. Demetalation and metalation protocol of DM-hCAII

For demetalation of DM-hCAII, a solution containing 200 mM sodium phosphate, 50 mM pyridine-2,6-dicarboxylic acid (PDA), pH 7, was added to the protein solution and incubated overnight at 4 °C. The apo-hCAII was buffer-exchanged to 10 mM HEPES, pH 6.8, using 10,000 MWCO Amicon centrifugation devices. Protein samples were in a water buffered solution with 10% D_2O, with a protein concentration around 350 μM.

The paramagnetic cobalt(II)-DM-hCAII samples were prepared by titrating the apo-DM-hCAII (350 μM in 10 mM HEPES, pH 6.8) sample with cobalt(II) sulfate solution. The procedure was followed by 1D ^{1}H and 2D ^{1}H—^{15}N HSQC spectra by monitoring the disappearance of the resonances of the apo-protein and the appearance of the paramagnetic resonances of the metalated protein at different chemical shift values. The titration was stopped when the resonances corresponding to the residues close to the paramagnetic center fully disappeared, and when the new resonances, at a different chemical shift, did not increase in intensity anymore. The same procedure was followed for the diamagnetic reference sample, where apo-DM-hCAII (350 μM in 10 mM HEPES, pH 6.8) was titrated with zinc(II) sulfate until the resonances matched the assignment of zinc(II)-WT-hCAII. After metalation, both protein solutions were buffer-exchanged to 10 mM HEPES pH 6.3, and increasing amounts of a solution of sodium thiocyanate were added to the protein samples (at the concentration of ~350 μM) in order to have 1:1.3, 1:2, 1:13, 1:1357 protein:ligand ratios. The protein/ligand ratios were chosen to be compared with previous studies reported in the literature [12].

2.4. NMR measurements

Solution 2D ^{1}H—^{15}N HSQC NMR spectra of ^{15}N isotopically enriched zinc(II)- and cobalt(II)-substituted DM-hCAII, for the evaluation of PCSs, were recorded on a Ascend™ 500 MHz BRUKER NMR Spectrometer equipped with a PRODIGY CryoProbe, and on a Ascend™ 1.2 GHz Bruker NMR Spectrometer, equipped with a TCI CryoProbe. Protein samples were prepared in a water buffered solution (10 mM HEPES, pH 6.3) and were titrated with sodium thiocyanate in order to achieve 1:1.3, 1:2, 1:13, 1:1357 protein:ligand ratios. All the spectra were processed with Bruker TopSpin software and analyzed with the program CARA [36].

The assignment of the diamagnetic zinc(II)- and paramagnetic cobalt (II)-DM-hCAII spectra was previously published [16]. The assignment of both metal forms in the presence of sodium thiocyanate was done by following the observed shifts during titration. The PCSs were calculated from the difference of the chemical shifts between the paramagnetic cobalt(II)- and diamagnetic zinc(II)-DM-hCAII spectra of the protein.

The ^{1}H—^{15}N RDC were measured at 298 K at 1.2 GHz Bruker NMR spectrometer, equipped with a TCI CryoProbe, for both metallic forms (at the concentration of 350 μM) reacted with 700 μM sodium thiocyanate.

2.5. Relaxation experiments

The experiments for the determination of the longitudinal and transverse relaxation rates (R_1 and R_2) and of the NOEs of the backbone ^{15}N nuclear spins were recorded at 298 K and at 700 MHz on ^{15}N enriched zinc(II)-DM-hCAII (at the concentration of 350 μM) [37,38]. Details on the applied pulse sequence are provided in the supporting information.

2.6. Pseudocontact shifts

The PCSs are described by the Kurland and McGarvey Eq. [39–41]:

$$\Delta\delta^{pcs} = \frac{1}{12\pi}\frac{1}{r^3}\left[\Delta\chi_{ax}\left(3cos^2\theta - 1\right) + \frac{3}{2}\Delta\chi_{rh}\, sin^2\theta cos(2\varphi)\right]$$

where r is the distance between the observed nuclear spin and the paramagnetic center; $\Delta\chi_{ax}$ and $\Delta\chi_{rh}$ are the axial and rhombic magnetic susceptibility anisotropies, respectively, θ is the angle between **r** and the z-axis of the magnetic susceptibility tensor, and φ is the angle between the projection of **r** on the xy plane and the x-axis [42].

2.7. Residual dipolar couplings

The paramagnetic RDCs, due to the partial alignment induced by a paramagnetic center present in the molecule, are given by [43,44]:

$$\Delta J_{ij}^{RDC}(Hz) = \frac{-B_0^2}{15kT}\frac{\gamma_i\gamma_j h}{16\pi^3 r_{ij}^3}\left[\Delta\chi_{ax}\left(3cos^2\alpha - 1\right) + \frac{3}{2}\Delta\chi_{rh} sin^2\alpha\, cos2\beta\right]$$

where $\Delta\chi_{ax}$ and $\Delta\chi_{rh}$ are the axial and rhombic magnetic susceptibility anisotropies, respectively, α is the angle between the internuclear vector and the z-axis of the magnetic susceptibility tensor, β is the angle between the projection of the internuclear vector on the xy plane and the x-axis, B_0 is the strength of the external magnetic field; γ_I and γ_j are the gyromagnetic ratios of the observed nuclei, and T is the temperature.

2.8. Electron paramagnetic resonance (EPR) measurements

EPR spectroscopy was performed using a Bruker EMX spectrometer equipped with an Oxford Instruments ESR-900, with a microwave frequency of 9.40 GHz, in a continuous flow helium cryostat, at 4 K, and a high sensitivity perpendicular mode rectangular cavity. The protein concentrations were 50 μM and sodium thiocyanate was added to have the same protein/ligand ratio used to acquire NMR experiments (1:1.3 and 1:1375). EPR spectra were fitted using the EasySpin [45] program to obtain the apparent g-values and the hyperfine coupling constants parameters.

2.9. Circular dichroism (CD) experiments

Circular dichroism spectra were recorded on a Chirascan™ qCD spectrometer. Each CD spectrum represents the average of five scans obtained by collecting data at 1 nm bandwidth. The spectra were collected in the 250–320 nm region using a 2 mm optical pathlength cuvette. Protein samples of zinc(II)-WT-hCAII were diluted to 1 mg/mL. The protein buffer consisted of 5 mM HEPES pH 6.3. The sodium thiocyanate ligand concentrations used were the following: 0 μM, 0.066 mM, 33.34 mM and 500 mM. Samples containing the pure ligand at the same concentrations were used as blank.

2.10. X-ray crystallography

The initial solutions of the metalated forms, cobalt(II)- and zinc(II)-DM-hCAII, had a concentration close to 15 mg/mL, in 10 mM HEPES, pH 6.8 buffer. Crystallization assays were performed using the sitting drop vapor diffusion method by mixing equal amounts of sample volume and of a solution containing 100 mM HEPES pH 7.5, 2.9 M ammonium sulphate and 1 mM 4-hydroxymercuric benzoic acid sodium salt. Cobalt (II)-DM-hCAII was crystallized using seeds from zinc(II)-DM-hCAII. Crystals for both metallic forms were soaked overnight with a solution containing 100 mM HEPES pH 6.3, 2.9 M ammonium sulfate, 1 mM 4-hydroxymercuric benzoic acid sodium salt and 500 mM sodium thiocyanate (1:1000 protein/ligand ratio).

X-ray diffraction data obtained for the crystal of zinc(II)-DM-hCAII were collected at UCIBIO, FCT-NOVA, using the in-house X-ray diffractometer (IμS 3.0 microfocus D8 Venture with copper K_α radiation), coupled to a CMOS Photon 100 detector, at 110 K, and with a maximum resolution of 1.75 Å. X-ray diffraction data from the crystal of cobalt(II)-DM-hCAII was collected at ALBA synchrotron using the XALOC beamline, with a maximum resolution of 1.46 Å.

Several software packages were used for the structure determination. The datasets were processed using PROTEUM3 software [46], the electron density maps were obtained using CCP4.The refinement of the obtained structures was done using the PHENIX suite [47], water molecules were added between refinement cycles, and the models were subjected to adjustments using COOT [48]. The X-ray structures of zinc (II)-DM-hCAII and cobalt(II)-DM-hCAII have been deposited in the Protein Data Bank under the accession codes 8OGD and 8OGE, respectively.

3. Results

3.1. EPR of cobalt(II)-DM-hCAII

The EPR spectra of cobalt(II)-DM-hCAII were collected in the absence and presence of sodium thiocyanate in 1:1.3 and 1:1357 protein:ligand ratios (Fig. 2). As previously observed for the bovine isoform [34], the spectra change with increasing concentration of sodium thiocyanate. When thiocyanate is added at the same concentration as the protein, it generated a class A spectrum, with g values around 6.8, 2.8 and 1.6. This is consistent with the presence of a 5-coordinated geometry around the cobalt(II) ion [49]. As previously reported, also the free protein gives a class A spectrum, but with less marked features [50]. Interestingly, the EPR spectrum of the cobalt(II)-DM-hCAII in the presence of equimolar concentration of thiocyanate shows a ^{59}Co hyperfine structure at low fields of the EPR spectrum. This may be attributed as coming from a better resolved EPR spectrum in the thiocyanate sample.

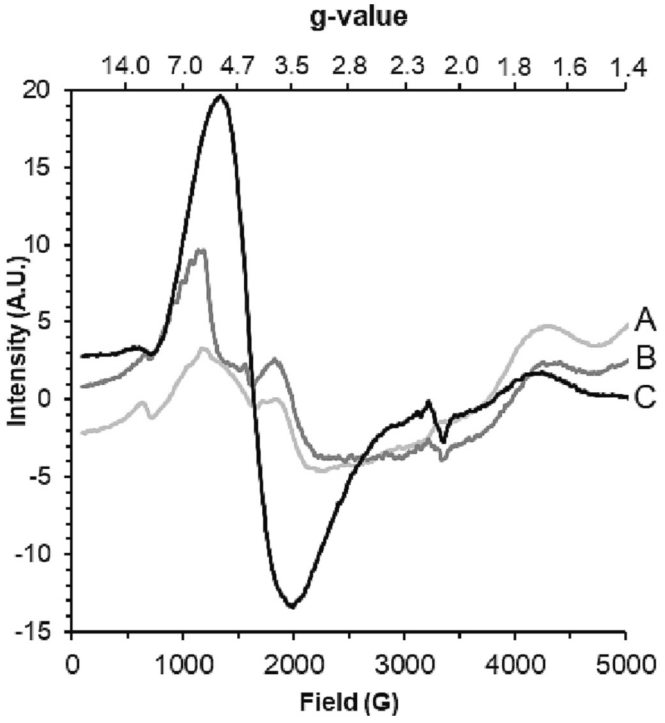

Fig. 2. EPR spectra of glassy aqueous solution of cobalt(II)-DM-hCAII in the absence and presence of increasing concentrations of sodium thiocyanate. A) Free-cobalt(II)-DM-hCAII B) cobalt(II)-DM-hCAII-thiocyanate (1:1.3); C) cobalt (II)-DM-hCAII-thiocyanate (1:1357). Spectra collected at 9.4 GHz at 4.0 Kelvin.

A well resolved ^{59}Co hyperfine splitting was also observed in the EPR spectrum of the complex with iodide [34]. On the other hand, when thiocyanate is added in large excess, the EPR spectrum changes dramatically, giving rise to a class C spectrum, with a g value around 4.0.

3.2. Paramagnetic NMR

Changes in the coordination environment of the cobalt(II) ion upon thiocyanate binding should result in changes in its magnetic susceptibility anisotropy, and thus on the observed PCSs [19,51–53]. ^{1}H—^{15}N HSQC spectra of ^{15}N-cobalt(II)-DM-hCAII and ^{15}N-zinc(II)-DM-hCAII were thus acquired in the presence of increasing amounts of the ligand, from 1:1.3 until thousand-fold ligand concentration, in order to measure ^{1}H and ^{15}N PCSs.

The spectra for the free cobalt(II)-DM-hCAII and zinc(II)-DM-hCAII proteins (Fig. S1 and S2) are very similar to those obtained in previous studies, so that the assignment of the spectra is mostly unchanged. In both proteins, the addition of sodium thiocyanate causes shifts of the nuclear resonances (Fig. S3 and S4), which change with the ligand concentration, indicating that this ligand interacts with both proteins. The chemical shift perturbation (CSP) analysis of zinc(II)-DM-hCAII indicates that the residues in the first coordination sphere (His 94, His 96 and His 119), in the second coordination sphere (Gln 92, Glu 117, Thr 199 and Asn 243) and some other neighboring residues are perturbed (see Fig. S8). Fig. S4 shows that some nuclear resonances of cobalt(II)-DM-hCAII shift by over 0.5 ppm upon ligand addition. However, the largest shifts occur immediately after the addition of a stoichiometric amount of the ligand.

From the differences between the nuclear resonance positions in the paramagnetic and in the diamagnetic proteins, PCSs were calculated and fitted with the program FANTEN [54] to determine the magnetic susceptibility anisotropy tensor $\Delta\chi$ at the different ligand concentrations. The fit was performed against the highest resolution (0.9 Å) structure of zinc(II)-WT-hCAII (PDB 3KS3) [1]. The agreement between the experimental and best-fit data is very good for all ligand concentrations, as shown in Fig. 3. Fig. 3 also shows the PCS isosurfaces and the tensor orientations with respect to the protein residues coordinated by the metal ion.

The best fit values for the axial and rhombic anisotropy components ($\Delta\chi_{ax}$ and $\Delta\chi_{rh}$) are reported in Table 1. It is apparent that there is a large increase in the anisotropy values from the free enzyme to the 1.3-fold thiocyanate sample. The change in the anisotropy values is accompanied by a sizable reorientation of the magnetic susceptibility tensor, as shown in Fig. 3. There is still a small increase in the anisotropy values with increasing the concentration of thiocyanate up to 1:13. The $\Delta\chi$ values then remain basically constant on passing from the 13-fold to the 1357-fold thiocyanate concentration, and also the tensor orientation does not significantly change, meaning that the coordination of the metal at the active center remains the same.

The magnetic susceptibility anisotropy tensors for the 1:2 sample were calculated also including paramagnetic RDC values in the fit performed with FANTEN [54]. Table S1 shows that the tensor anisotropies are similar when calculated using PCS alone, RDC alone, or PCS and RDC.

Comparing the $\Delta\chi$ tensors obtained for different ligands (oxalate, furosemide and thiocyanate, Table 1) of cobalt(II)-hCAII, we observe that furosemide provides the lowest axial and rhombic anisotropy, which indicates that the tetra-coordinated geometry of the free cobalt (II)-hCAII is maintained also in the presence of this ligand [16]. Conversely, $\Delta\chi_{ax}$ and $\Delta\chi_{rh}$ increase to values typical of a penta-coordinated geometry [7,16,32,55] in the presence of oxalate or thiocyanate.

3.3. X-ray crystallography

A 5-coordination geometry of the thiocyanate adduct is confirmed by

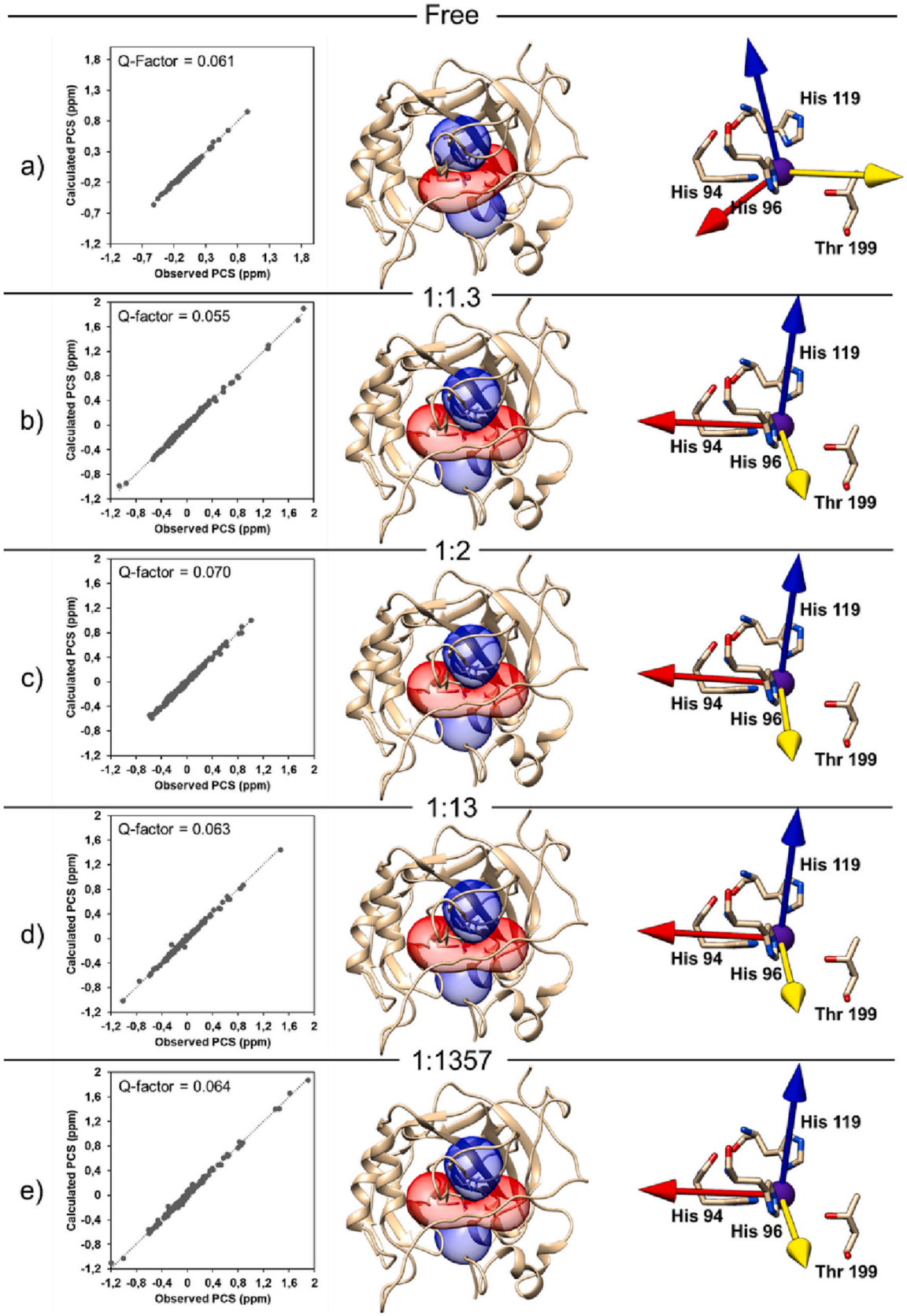

Fig. 3. Correlation plots between experimental and calculated PCS and respective representation of the PCS surfaces 1 (blue) and − 1 (red) and the magnetic susceptibility anisotropy main axis directions in the absence and presence of different concentrations of sodium thiocyanate at pH 6.3. a) Free cobalt(II)-DM-hCAII; b) cobalt(II)-DM-hCAII-thiocyanate 1:1.3; c) cobalt(II)-DM-hCAII-thiocyanate 1:2; d) cobalt(II)-DM-hCAII-thiocyanate 1:13; e) cobalt(II)-DM-hCAII-thiocyanate 1:1357. (For interpretation of the references to colour in this figure legend, the reader is referred to the web version of this article.)

Table 1
Magnetic susceptibility tensor anisotropy parameters calculated with the program FANTEN for adducts of cobalt(II)-DM-hCAII and cobalt(II)-WT-hCAII.

	Ligand	pH	$\Delta\chi_{ax}$ (10^{-32} m^3)	$\Delta\chi_{rh}$ (10^{-32} m^3)	Q-factor	Number of PCS	
DM-hCAII	No	6.0	3.23 ± 0.01	−1.10 ± 0.02	0.062	169	
DM-hCAII	No	6.3	3.15 ± 0.02	−0.59 ± 0.02	0.061	161	
DM-hCAII	Thiocyanate (1.3-fold)	6.3	6.71 ± 0.05	−2.30 ± 0.03	0.055	157	
DM-hCAII	Thiocyanate (2-fold)	6.3	7.41 ± 0.05	−2.81 ± 0.04	0.070	150	
DM-hCAII	Thiocyanate (13-fold)	6.3	7.76 ± 0.04	−2.95 ± 0.05	0.063	141	
DM-hCAII	Thiocyanate (1357-fold)	6.3	7.69 ± 0.04	−2.95 ± 0.06	0.064	143	
WT-hCAII	Oxalate	5.8	6.54 ± 0.04	−4.44 ± 0.03	0.07	160	[16]
WT-hCAII	Furosemide	6.8	3.09 ± 0.02	−1.69 ± 0.02	0.07	174	[16]

X-ray crystallography. Crystallographic data for zinc(II)-WT-hCAII (PDB 2CA2 [56] and 4YGK [49]) and its T199P/C206S mutant (PDB 1LG6 [57]) show that the zinc(II) ion is bound to three protein histidine side-chains, one water molecule and one thiocyanate anion. To confirm this coordination geometry also for the zinc(II) and cobalt(II)-DM-hCAII at high ligand concentrations, we successfully crystallized the two proteins (Fig. S10) and determined their crystal structures. Crystals of free protein were soaked overnight with a concentrated solution of thiocyanate (1:1000 protein/ligand ratio).

The structures of zinc(II)-DM-hCAII-thiocyanate and cobalt(II)-DM-hCAII-thiocyanate were solved using the molecular replacement method, using as search model the highest diffracting structure of zinc (II)-WT-hCAII (PDB 3K34) with a maximum resolution of 1.75 Å and 1.46 Å, respectively. The relevant data collection and refinement statistics are shown in Table S2**.** The structures of cobalt(II)-DM-hCAII and zinc(II)-DM-hCAII were compared with the deposited highest resolution structure of hCAII bound to thiocyanate (4YGK) [49] and resulted in very good agreement (Fig. 4 and Table S3), proving that the mutations of DM-hCAII do not affect the overall structure of hCAII. For both proteins, the metal ions are coordinated by five ligands, that are: the Nε_2 from His-94 (distant 2.1 Å from both metal ions); the Nε_2 from His-96 (distant 2.0 and 2.2 Å from the metal ion, in cobalt(II)-DM-hCAII and zinc(II)-DM-hCAII, respectively); the Nδ_1 from His-119 (distant 2.1 and 2.2 Å from the metal ion, in cobalt(II)-DM-hCAII and zinc(II)-DM-hCAII, respectively); the nitrogen's thiocyanate (distant 2.0 Å from both metal ions); the oxygen of a water molecule (distant 2.1 and 2.2 Å from the metal ion, in cobalt(II)-DM-hCAII and zinc(II)-DM-hCAII, respectively). The anomalous signal arising from the active center of cobalt(II)-DM-hCAII-SCN^- confirmed the presence of the cobalt(II) ion in the active center of the protein (Fig. S11). Furthermore, as expected, the structure of hCAII does not change with the replacement of the zinc(II) ion with the cobalt (II) ion in the active site.

For comparison purposes the X-ray structure of the free cobalt(II)-DM-hCAII was solved. The active site structure clearly shows that the cobalt(II) ion is coordinated by three protein histidine ligands and by two water molecules. In particular, the ligands are: the Nε_2 from His-94, the Nε_2 from His-96 and the Nδ_1 from His-119 (the nitrogen atoms of all the three histidine residues are 2.2 Å apart from the metal ion); the fourth and fifth ligands, instead, are oxygens from two water molecules (2.1 and 2.7 Å apart from the metal ion).

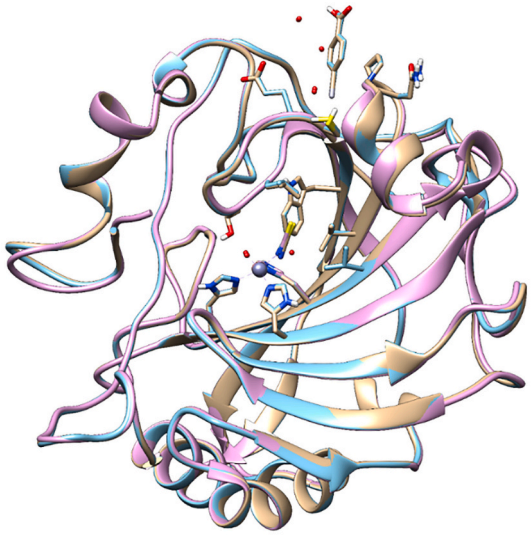

Fig. 4. Cartoon representation of zinc(II)-WT-hCAII-thiocyanate (purple, PDB 4YGK, 1.5 Å); zinc(II)-DM-hCAII-thiocyanate (cream, 1.75 Å) and cobalt(II)-DM-hCAII-thiocyanate (light blue, 1.46 Å). (For interpretation of the references to colour in this figure legend, the reader is referred to the web version of this article.)

3.4. Circular dichroism measurements of zinc(II)-DM-hCAII

CD spectra were collected to monitor whether the global and the secondary structure of the protein is maintained in the presence of a large amount of thiocyanate, a chaotropic agent that might denature it. Since sodium thiocyanate absorbs in the 200–250 nm range, CD spectra were acquired in the range between 250 and 320 nm in the near-UV region. This range is informative regarding the chemical environment of the aromatic protein residues (histidine, tyrosine and tryptophan). Indeed, the tryptophan residues have been shown to provide a dominant contribution to the spectrum in the whole region [58]. Fig. 5 shows that for any of the tested concentrations of sodium thiocyanate, up to 1000-fold excess, the CD spectra do not change appreciably with respect to the free enzyme, thus indicating that the environment of the protein aromatic residues remained unchanged. Since many of the protein tryptophan residues are in the hydrophobic core of the protein, it is possible to conclude that the protein core structure does not change.

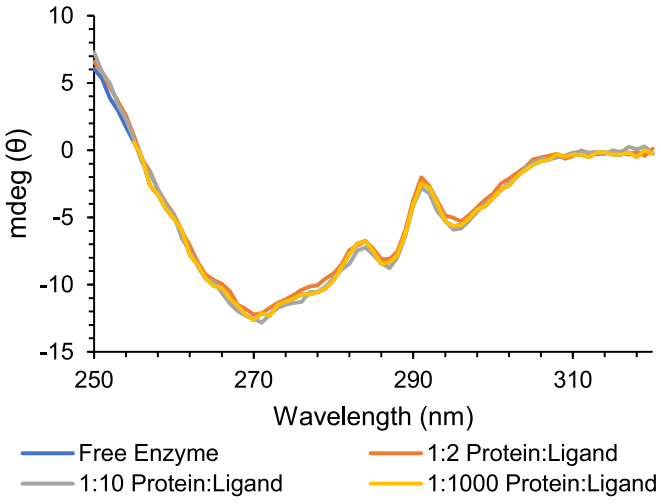

Fig. 5. Circular dichroism spectra in the Near-UV range of zinc(II)-WT-hCAII free and bound to increasing concentrations of sodium thiocyanate.

3.5. NMR relaxation measurements of zinc(II)-DM-hCAII

^{15}N NMR relaxation studies were performed to study the effect of thiocyanate on the overall dynamics of the zinc(II)-DM-hCAII protein [37,38,59]. The experimental data were compared to the values calculated with the program HYDRONMR [60], which calculates R_1 and R_2 from the protein structure assumed as rigid, that is neglecting possible local mobility.

Fig. 6 shows the experimental R_1, R_2 and NOE values obtained for the amide ^{15}N nuclei of zinc(II)-DM-hCAII in the absence and in the presence of different concentrations of sodium thiocyanate. In all cases, the experimental R_1 values are higher and the experimental R_2 values are lower than those predicted by HYDRONMR, using a crystal structure PDB 3KS3, thus pointing out to some internal mobility. At a 1:2 protein: ligand ratio, the R_1, R_2, and NOE values do not change appreciably with respect to the values measured without the ligand. At 1000-fold excess of thiocyanate, the R_1 values undergo a modest decrease to values closer to the calculated ones, the R_2 values do not change appreciably, and the NOE values are more disperse. Table 2 shows the average R_1 and R_2 values and the derived isotropic rotational correlation times (τ_c^{iso}).

Table 2
Calculated global average ^{15}N relaxation rate parameters R_1 and R_2 with respective standard deviation and correlation time (τ_c) of zinc(II)-DM-hCAII (475 μM) aqueous solutions in the absence and presence of increasing concentrations of sodium thiocyanate.

	Free enzyme	1:2 ratio	1:1357 ratio
R_1 (s^{-1})	1.2 ± 0.1	1.2 ± 0.1	0.8 ± 0.1
R_2 (s^{-1})	20 ± 2	20 ± 2	20 ± 2
τ_c^{iso} (ns)	10.9 ± 0.5	10.9 ± 0.5	13.2 ± 0.6

4. Discussion

Fig. 7 summarises in a qualitative way the main results obtained using several experimental techniques applied to the free protein, the protein in the presence of stoichiometric amounts of thiocyanate, and the protein in thousand-fold excess of thiocyanate. The results are seemingly contradictory: as judged from the EPR spectra, while the stoichiometric addition of thiocyanate causes modest changes in the spectral features, a dramatic change occurs with large excess of thiocyanate; as judged from the paramagnetic NMR data, a dramatic change occurs in the presence of stoichiometric amounts of thiocyanate, while a thousand-fold excess essentially does not cause further alterations.

It is well known that the cobalt(II) ion in the pure enzyme is essentially in a pseudotetrahedral coordination [7,61,62], while the thiocyanate adduct is five-coordinated. The paramagnetic NMR data are perfectly consistent with these coordination geometries, the magnetic susceptibility anisotropy values being much smaller in the pure enzyme than in the thiocyanate derivative. Therefore, the sketch reported in Fig. 7 for the NMR results can be read as the cobalt(II) center passing from a pseudotetrahedral geometry to a five-coordinated geometry upon binding of stoichiometric amount of thiocyanate, and then essentially remaining five-coordinated under further additions of the ligand.

By using a similar correlation between spectral features and coordination geometry for the EPR data, one should envision a five-coordinated cobalt(II) center also for the free protein, the metal remaining five-coordinated upon addition of stoichiometric amounts of thiocyanate, and then possibly moving to a six-coordinated center when thiocyanate is in large excess. The latter coordination change is likely to be achieved by a global effect on the protein structure by a modification of the frozen solvent glass when a large excess of thiocyanate is present. We should also point out that the differences in the coordination geometry of the free enzyme observed by EPR and NMR measurements cannot be explained by possible differences in the pH values used for the collection of the experiments. Indeed, the low temperature used to collect EPR data (4 K) could cause an increase in pH. However, high pH (9.5) favors four-coordination geometry for cobalt(II)-hCAII, whereas low pH (5.8) promotes the formation of five-coordinated complexes, as previously reported [7], thus leading to an opposite effect with respect to what is observed here.

The X-ray data recorded in the present work for the thiocyanate complex seem to agree with both the EPR and the NMR data (Fig. 7), showing five-coordination (three histidines, one thiocyanate ion and one water molecule). Previous reports on the free cobalt protein suggests the presence of a significant amount of a five coordinated cobalt(II) complex (three histidines and two water molecules) [10], i.e. more in agreement with the EPR data.

Of the three techniques, however, paramagnetic NMR is the only technique which is applicable to the protein in solution at room temperature. EPR is performed on a glassy solution at around liquid helium temperature and X-ray is performed on crystals at approximately liquid nitrogen temperature. Therefore, the most likely explanation for the discrepancies among the different techniques is that lowering the temperature favors the binding of a second water molecule in the free enzyme. The difference is therefore not in the structure of the thiocyanate complex but in the structure of the free enzyme, which shifts from four to five coordination at low temperature. It should be recalled that an equilibrium between four and five coordination for the free enzyme has already been proposed at room temperature and low pH, so a relatively minor change in the enthalpy/entropy balance would be

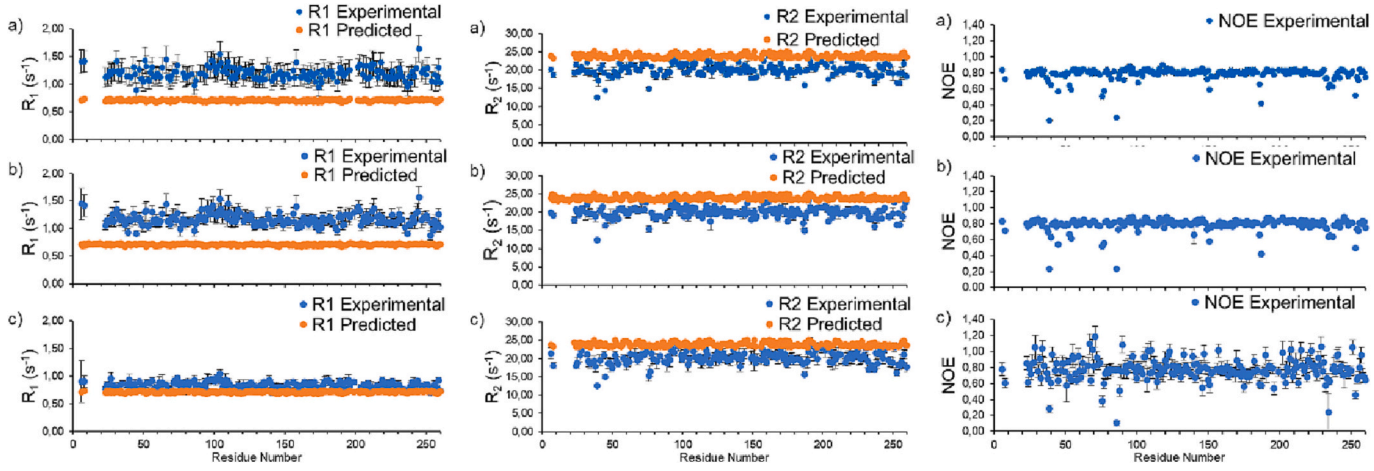

Fig. 6. Backbone ^{15}N experimental and predicted (HYDRONMR) [60] R_1, R_2 and NOE vs residue number at different sodium thiocyanate concentrations: a) Free zinc (II)-DM-hCAII; b) 1:1.3 protein:sodium thiocyanate ratio and c) 1:1357 protein:sodium thiocyanate ratio.

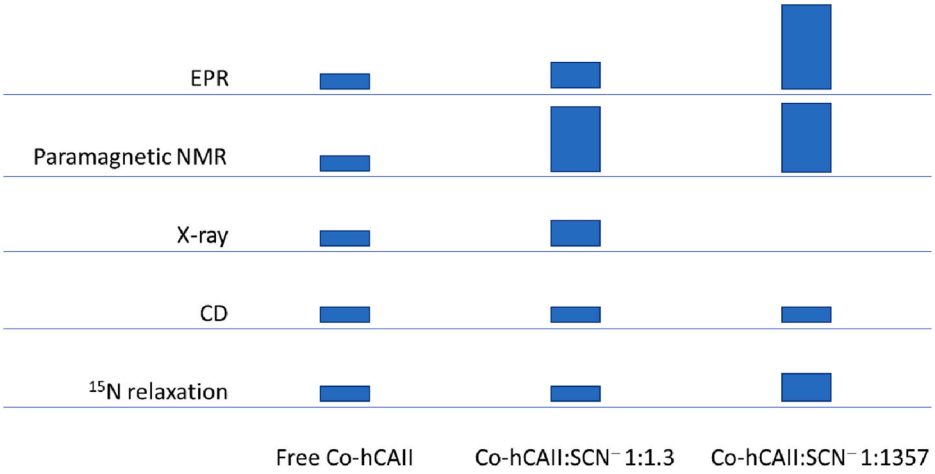

Fig. 7. Qualitative summary of the changes measured by the various experimental techniques for the free protein, the protein in the presence of stoichiometric amounts of thiocyanate, and the protein in thousand-fold excess of thiocyanate. The EPR data were acquired at 4 K, the X-ray at 110 K, and the NMR and CD at 298 K. The blue bars qualitatively reflect the observables of the different techniques, that are: the g-tensors values, for EPR; the axial and rhombic components of the magnetic susceptibility anisotropy tensor, for paramagnetic NMR; the coordination geometry of the metal, for X-ray; the global structure of the protein, for CD; the R_1 values for ^{15}N relaxation. (For interpretation of the references to colour in this figure legend, the reader is referred to the web version of this article.)

sufficient. It remains to be explained why a large excess of thiocyanate causes a change towards a more axial EPR spectrum, suggestive of a six-coordinated metal environment, while this is not observed in the NMR at room temperature.

Thiocyanate is known to be a chaotropic agent, potentially able to destroy or at least grossly alter the tertiary structure of a protein. CD spectra clearly show that this is not the case, as they remain essentially identical from the free enzyme to stoichiometric addition of thiocyanate to large excess of thiocyanate (Fig. 7). Consistently, crystals for X-ray survived after overnight soaking at room temperature with 500 mM thiocyanate, indicating that no major alterations of the overall 3D structure of the protein occurs. While soaking with 500 mM thiocyanate for a short time does not show appreciable amounts of thiocyanate in the crystal lattice, soaking for a long time results in breaking of the crystals, as expected from excessive penetration of thiocyanate in the crystal lattice. As a further and more sensitive test of the possible chaotropic effects of thiocyanate, we performed ^{15}N NMR relaxation measurements on the zinc(II) derivative. As described in the Results section and summarized in Fig. 7, the relaxation parameters do not change between free enzyme and stoichiometric amounts of thiocyanate, while they only change modestly in the presence of large excess of thiocyanate. The modest increase in the rotational correlation time in the latter case suggests a slight swelling of the protein, possibly due to the binding of several thiocyanate ions on the surface. An interesting additional feature of the high thiocyanate concentration sample is the significant scattering of the NOE data, that may indicate that several local changes in the backbone mobility may occur. In any case, the paramagnetic NMR data indicate that these changes do not affect at all the coordination geometry of the metal.

We may conclude that the dramatic change occurring in the EPR spectra in large excess of thiocyanate are due to a combination of the chaotropic effect, which at room temperature is present but apparently modest, with the low temperature of the EPR measurements, possibly coupled with a change in the nature of the glassy solution that might cause distortions of the three dimensional structure and partial opening of the active site, allowing for the coordination of a further water molecule.

Author statement

CL, ALM, CFGCG and ER designed the project; JMS, LC, ALC and MF performed all experiments and compiled the data; all authors interpreted and discussed the data; JMS, GP and CL drafted the paper and all authors continued to write, edit and review the manuscript together. All authors have read and agreed to the published version of the manuscript.

Declaration of Competing Interest

The authors declare that they have no known competing financial interests or personal relationships that could have appeared to influence the work reported in this paper.

Data availability

Data will be made available on request.

Acknowledgements

This work has been supported by the Fondazione Cassa di Risparmio di Firenze. NMR measurements performed at 1200 MHz spectrometer were done with the support and the use of resources of Instruct-ERIC, a landmark ESFRI project, and specifically the CERM/CIRMMP Italy center. This work was supported by Fundação para a Ciência e a Tecnologia (FCT-Portugal) for funding UCIBIO project (UIDP/04378/2020 and UIDB/04378/2020) and Associate Laboratory Institute for Health and Bioeconomy – i4HB Project (LA/P/0140/2020). The authors also thank FCT-Portugal for the Ph.D. grant awarded to José Malanho Silva (PD/BD/135180/2017) under the PTNMRPhD Program - NMR applied to chemistry, materials, and biosciences (PD/00065/2013). The authors acknowledge the ALBA synchrotron facility (Barcelona, Spain) for access to the BL-13 XALOC beamline. This work was supported by the Portuguese Foundation for Science and Technology (FCT-MCTES) through the Applied Molecular Biosciences Unit (UCIBIO) grant UIDB/04378/2020. Also, through national project grant RECI/BBB-BEP/0124/2012 that financed the X-Ray Diffraction facility of UCIBIO. The 500 MHz NMR spectrometer used in the experiments is part of the National NMR Facility supported by FCT-Portugal (ROTEIRO/0031/2013–PIN-FRA/22161/2016, co-financed by FEDER through COMPETE 2020, POCI, and PORL and FCT through PIDDAC). C.F.G.C.G. is grateful to the Fundação para a Ciência e a Tecnologia (FCT) for funding of CQC-IMS through projects UIDB/00313/2020 and UIDP/00313/2020.

Appendix A. Supplementary data

Supplementary data to this article can be found online at https://doi.org/10.1016/j.jinorgbio.2023.112222.

References

[1] B.S. Avvaru, C.U. Kim, K.H. Sippel, S.M. Gruner, M. Agbandje-McKenna, D. N. Silverman, R. McKenna, A short, strong hydrogen bond in the active site of human carbonic anhydrase II, Biochemistry. 49 (2010) 249–251, https://doi.org/10.1021/bi902007b.

[2] K.K. Sethi, D. Vullo, S.M. Verma, M. Tanç, F. Carta, C.T. Supuran, Carbonic anhydrase inhibitors: synthesis and inhibition of the human carbonic anhydrase isoforms I, II, VII, IX and XII with benzene sulfonamides incorporating 4,5,6,7-tetrabromophthalimide moiety, Bioorg. Med. Chem. 21 (2013) 5973–5982, https://doi.org/10.1016/j.bmc.2013.07.044.

[3] C.B. Mishra, M. Tiwari, C.T. Supuran, Progress in the development of human carbonic anhydrase inhibitors and their pharmacological applications: where are we today? Med. Res. Rev. 40 (2020) 2485–2565, https://doi.org/10.1002/med.21713.

[4] A.S. Lipton, R.W. Heck, P.D. Ellis, Zinc solid-state NMR spectroscopy of human carbonic anhydrase: implications for the enzymatic mechanism, J. Am. Chem. Soc. 126 (2004) 4735–4739, https://doi.org/10.1021/ja0305609.

[5] K. Hakansson, A. Wehnert, A. Liljas, X-ray analysis of metal-substituted human carbonic anhydrase II derivatives, Acta Crystallogr. D Biol. Crystallogr. 50 (1994) 93–100, https://doi.org/10.1107/S0907444993008790.

[6] J.E. Coleman, Mechanism of action of carbonic anhydrase, J. Biol. Chem. 242 (1967) 5212–5219, https://doi.org/10.1016/S0021-9258(18)99413-5.

[7] I. Bertini, C. Luchinat, Cobalt(II) as a probe of the structure and function of carbonic anhydrase, Acc. Chem. Res. 16 (1983) 272–279, https://doi.org/10.1021/ar00092a002.

[8] J. Malanho Silva, L. Cerofolini, S. Giuntini, V. Calderone, C.F.G.C. Geraldes, A. L. Macedo, G. Parigi, M. Fragai, E. Ravera, C. Luchinat, Metal centers in biomolecular solid-state NMR, J. Struct. Biol. 206 (2019) 99–109, https://doi.org/10.1016/j.jsb.2018.11.013.

[9] J.M. Silva, S. Giuntini, L. Cerofolini, C.F.G.C. Geraldes, A.L. Macedo, E. Ravera, M. Fragai, C. Luchinat, V. Calderone, Non-crystallographic symmetry in proteins: Jahn–teller-like and butterfly-like effects? JBIC J. Biol. Inorg. Chem. 24 (2019) 91–101, https://doi.org/10.1007/s00775-018-1630-0.

[10] B.S. Avvaru, D.J. Arenas, C. Tu, D.B. Tanner, R. McKenna, D.N. Silverman, Comparison of solution and crystal properties of co(II)–substituted human carbonic anhydrase II, Arch. Biochem. Biophys. 502 (2010) 53–59, https://doi.org/10.1016/j.abb.2010.07.010.

[11] I. Bertini, E. Borghi, C. Luchinat, R. Monnanni, Nickel carbonic anhydrase: a re-examination of the electronic spectra with the help of CD spectra, Inorg. Chim. Acta 67 (1982) 99–102, https://doi.org/10.1016/S0020-1693(00)85049-5.

[12] I. Bertini, G. Canti, C. Luchinat, A. Scozzafava, Characterization of cobalt(II) bovine carbonic anhydrase and of its derivatives, J. Am. Chem. Soc. 100 (1978) 4873–4877, https://doi.org/10.1021/ja00483a038.

[13] I. Bertini, C. Luchinat, The structure of cobalt(II)-substituted carbonic anhydrase and its implications for the catalytic mechanism of the enzyme, Ann. N. Y. Acad. Sci. 429 (1984) 89–98, https://doi.org/10.1111/j.1749-6632.1984.tb12318.x.

[14] L. Cerofolini, J.M. Silva, E. Ravera, M. Romanelli, C.F.G.C. Geraldes, A.L. Macedo, M. Fragai, G. Parigi, C. Luchinat, How do nuclei couple to the magnetic moment of a paramagnetic center? A new theory at the gauntlet of the experiments, J. Phys. Chem. Lett. 10 (2019) 3610–3614, https://doi.org/10.1021/acs.jpclett.9b01128.

[15] I. Bertini, G. Canti, C. Luchinat, Water in the coordination sphere of metallocarbonic anhydrases: a solvent proton longitudinal relaxation study at several frequencies, Inorg. Chim. Acta 56 (1981) 99–107, https://doi.org/10.1016/S0020-1693(00)88554-0.

[16] L. Cerofolini, T. Staderini, S. Giuntini, E. Ravera, M. Fragai, G. Parigi, R. Pierattelli, C. Luchinat, Long-range paramagnetic NMR data can provide a closer look on metal coordination in metalloproteins, J. Biol. Inorg. Chem. 23 (2018) 71–80, https://doi.org/10.1007/s00775-017-1511-y.

[17] C. Nitsche, G. Otting, Pseudocontact shifts in biomolecular NMR using paramagnetic metal tags, Prog. Nucl. Magn. Reson. Spectrosc. 98–99 (2017) 20–49, https://doi.org/10.1016/j.pnmrs.2016.11.001.

[18] P.H.J. Keizers, M. Ubbink, Paramagnetic tagging for protein structure and dynamics analysis, Prog Nucl Magn Reson, Spectrosc. 58 (2011) 88–96.

[19] E. Ravera, L. Gigli, L. Fiorucci, C. Luchinat, G. Parigi, The evolution of paramagnetic NMR as a tool in structural biology, Phys. Chem. Chem. Phys. 24 (2022) 17397–17416, https://doi.org/10.1039/D2CP01838A.

[20] G. Parigi, E. Ravera, C. Luchinat, Paramagnetic effects in NMR for protein structures and ensembles: studies of metalloproteins, Curr. Opin. Struct. Biol. 74 (2022), 102386, https://doi.org/10.1016/j.sbi.2022.102386.

[21] C.O. Fernandez, T. Niizeki, T. Kohzuma, A.J. Vila, Metal-ligand interactions in perturbed blue copper sites: a paramagnetic (1)H NMR study of co(II)-pseudoazurin, J.Biol.Inorg.Chem. 8 (2003) 75–82.

[22] T. Müntener, D. Joss, D. Häussinger, S. Hiller, Pseudocontact shifts in biomolecular NMR spectroscopy, Chem. Rev. 122 (2022) 9422–9467, https://doi.org/10.1021/acs.chemrev.1c00796.

[23] D. Parker, E.A. Suturina, I. Kuprov, N.F. Chilton, How the ligand field in lanthanide coordination complexes determines magnetic susceptibility anisotropy, paramagnetic NMR shift, and relaxation behavior, Acc. Chem. Res. 53 (2020) 1520–1534, https://doi.org/10.1021/acs.accounts.0c00275.

[24] E.A. Suturina, K. Mason, C.F.G.C. Geraldes, I. Kuprov, D. Parker, Beyond Bleaney's theory: experimental and theoretical analysis of periodic trends in lanthanide-induced chemical shift, Angew. Chem. 129 (2017) 12383–12386, https://doi.org/10.1002/ange.201706931.

[25] X.-C. Su, J.-L. Chen, Site-specific tagging of proteins with paramagnetic ions for determination of protein structures in solution and in cells, Acc. Chem. Res. 52 (2019) 1675–1686, https://doi.org/10.1021/acs.accounts.9b00132.

[26] B.-B. Pan, F. Yang, Y. Ye, Q. Wu, C. Li, T. Huber, X.-C. Su, 3D structure determination of a protein in living cells using paramagnetic NMR spectroscopy, Chem. Commun. (Camb.) 52 (2016) 10237–10240, https://doi.org/10.1039/c6cc05490k.

[27] F.A. Walker, Magnetic spectroscopic (EPR, ESEEM, Mössbauer, MCD and NMR) studies of low-spin ferriheme centers and their corresponding heme proteins, Coord. Chem. Rev. 185–186 (1999) 471–534, https://doi.org/10.1016/S0010-8545(99)00029-6.

[28] I. Bertini, C. Luchinat, G. Parigi, F.A. Walker, Heme methyl 1H chemical shifts as structural parameters in some low spin ferriheme proteins, J.Biol.Inorg.Chem. 4 (1999) 515–519.

[29] F.A. Walker, The heme environment of mouse neuroglobin: histidine imidazole plane orientations obtained from solution NMR and EPR spectroscopy as compared with X-ray crystallography, J. Biol. Inorg. Chem. 11 (2006) 391–397, https://doi.org/10.1007/s00775-006-0095-8.

[30] N.V. Shokhirev, F.A. Walker, The effect of axial ligand plane orientation on the contact and pseudocontact shifts of low-spin ferriheme proteins, JBIC. 3 (1998) 581–594, https://doi.org/10.1007/s007750050271.

[31] L. Banci, L.B. Dugad, G.N. La Mar, K.A. Keating, C. Luchinat, R. Pierattelli, 1H nuclear magnetic resonance investigation of cobalt(II) substituted carbonic anhydrase, Biophys. J. 63 (1992) 530–543, https://doi.org/10.1016/S0006-3495(92)81607-7.

[32] I. Bertini, B.H.B.H. Jonsson, C. Luchinat, R. Pierattelli, A.J.A.J. Vila, R. Plerattelli, A.J.A.J. Vila, Strategies of signal assignments in paramagnetic metalloproteins. An NMR investigation of the thiocyanate adduct of the cobalt(II)-substituted human carbonic anhydrase II, J. Magn. Reson. Ser. B 104 (1994) 230–239, https://doi.org/10.1006/jmrb.1994.1080.

[33] L. Cerofolini, S. Giuntini, A. Louka, E. Ravera, M. Fragai, C. Luchinat, High-resolution solid-state NMR characterization of ligand binding to a protein immobilized in a silica matrix, J. Phys. Chem. B 121 (2017) 8094–8101, https://doi.org/10.1021/acs.jpcb.7b05679.

[34] A. Bencini, I. Bertini, G. Canti, D. Gatteschi, C. Luchinat, The epr spectra of the inhibitor derivatives of cobalt carbonic anhydrase, J. Inorg. Biochem. 14 (1981) 81–93, https://doi.org/10.1016/S0162-0134(00)80016-1.

[35] H. Song, A.C. Weitz, M.P. Hendrich, E.A. Lewis, J.P. Emerson, Building reactive copper centers in human carbonic anhydrase II, J. Biol. Inorg. Chem. 18 (2013) 595–598, https://doi.org/10.1007/s00775-013-1009-1.

[36] R. Keller, The Computer Aided Resonance Assignment Tutorial, 2004.

[37] J. Cavanagh, Protein NMR Spectroscopy : Principles and Practice, 2007, p. 885.

[38] M. Gairí, A. Dyachenko, M.T. González, M. Feliz, M. Pons, E. Giralt, An optimized method for 15N R1 relaxation rate measurements in non-deuterated proteins, J. Biomol. NMR 62 (2015) 209–220, https://doi.org/10.1007/s10858-015-9937-4.

[39] R.J. Kurland, B.R. McGarvey, Isotropic NMR shifts in transition metal complexes: the calculation of the Fermi contact and pseudocontact terms, J. Magn. Reson. 2 (1970) (1969) 286–301, https://doi.org/10.1016/0022-2364(70)90100-9.

[40] L. Lang, E. Ravera, G. Parigi, C. Luchinat, F. Neese, Solution of a puzzle: high-level quantum-chemical treatment of Pseudocontact chemical shifts confirms classic Semiempirical theory, J. Phys. Chem. Lett. 11 (2020) 8735–8744, https://doi.org/10.1021/acs.jpclett.0c02462.

[41] L. Lang, E. Ravera, G. Parigi, C. Luchinat, F. Neese, Theoretical analysis of the long-distance limit of NMR chemical shieldings, J. Chem. Phys. 156 (2022), 154115, https://doi.org/10.1063/5.0088162.

[42] I. Bertini, C. Luchinat, G. Parigi, E. Ravera, NMR of Paramagnetic Molecules. Applications to Metallobiomolecules and Models, 2016.

[43] J.R. Tolman, J.M. Flanagan, M.A. Kennedy, J.H. Prestegard, Nuclear magnetic dipole interactions in field-oriented proteins: information for structure determination in solution, Proc. Natl. Acad. Sci. U. S. A. 92 (1995) 9279–9283.

[44] G. Parigi, E. Ravera, C. Luchinat, Magnetic susceptibility and paramagnetism-based NMR, Prog. Nucl. Magn. Reson. Spectrosc. 114–115 (2019) 211–236, https://doi.org/10.1016/j.pnmrs.2019.06.003.

[45] S. Stoll, A. Schweiger, EasySpin, a comprehensive software package for spectral simulation and analysis in EPR, J. Magn. Reson. 178 (2006) 42–55, https://doi.org/10.1016/j.jmr.2005.08.013.

[46] DOC-M86-EXX242 PROTEUM3 Software User Manual, Bruker AXS Inc., 2017.

[47] D. Liebschner, P.V. Afonine, M.L. Baker, G. Bunkoczi, V.B. Chen, T.I. Croll, B. Hintze, L.W. Hung, S. Jain, A.J. McCoy, N.W. Moriarty, R.D. Oeffner, B.K. Poon, M.G. Prisant, R.J. Read, J.S. Richardson, D.C. Richardson, M.D. Sammito, O. V. Sobolev, D.H. Stockwell, T.C. Terwilliger, A.G. Urzhumtsev, L.L. Videau, C. J. Williams, P.D. Adams, Macromolecular structure determination using X-rays, neutrons and electrons: recent developments in Phenix, Acta Crystallographica section D, Struct. Biol. 75 (2019) 861–877, https://doi.org/10.1107/S2059798319011471.

[48] P. Emsley, K. Cowtan, Coot : model-building tools for molecular graphics, Acta Crystallogr. D Biol. Crystallogr. 60 (2004) 2126–2132, https://doi.org/10.1107/S0907444904019158.

[49] J.M. Fox, K. Kang, W. Sherman, A. Héroux, G.M. Sastry, M. Baghbanzadeh, M. R. Lockett, G.M. Whitesides, Interactions between Hofmeister anions and the binding pocket of a protein, J. Am. Chem. Soc. 137 (2015) 3859–3866, https://doi.org/10.1021/JACS.5B00187.

[50] E. Grell, R.C. Bray, Electron paramagnetic resonance spectroscopy of bovine cobalt carbonic anhydrase B, Biochimica et Biophysica Acta (BBA) - protein, Structure. 236 (1971) 503–506, https://doi.org/10.1016/0005-2795(71)90232-7.

[51] L. Benda, J. Mareš, E. Ravera, G. Parigi, C. Luchinat, M. Kaupp, J. Vaara, Pseudocontact NMR shifts over the paramagnetic Metalloprotein CoMMP-12 from first principles, Angew. Chem. Int. Ed. Eng. 55 (2016) 14713–14717, https://doi.org/10.1002/anie.201608829.

[52] E. Ravera, L. Gigli, E.A. Suturina, V. Calderone, M. Fragai, G. Parigi, C. Luchinat, A high-resolution view of the coordination environment in a paramagnetic Metalloprotein from its magnetic properties, Angew. Chem. Int. Ed. 60 (2021) 14960–14966, https://doi.org/10.1002/anie.202101149.

[53] E. Ravera, L. Gigli, B. Czarniecki, L. Lang, R. Kümmerle, G. Parigi, M. Piccioli, F. Neese, C. Luchinat, A quantum chemistry view on two archetypical paramagnetic pentacoordinate nickel(II) complexes offers a fresh look on their NMR spectra, Inorg. Chem. 60 (2021) 2068–2075, https://doi.org/10.1021/acs.inorgchem.0c03635.
[54] M. Rinaldelli, A. Carlon, E. Ravera, G. Parigi, C. Luchinat, FANTEN: a new web-based interface for the analysis of magnetic anisotropy-induced NMR data, J. Biomol. NMR (2015), https://doi.org/10.1007/s10858-014-9877-4.
[55] I. Bertini, C. Luchinat, The reaction pathways of zinc enzymes and related biological catalysts, Bioinorg. Chem. 37–106 (1994).
[56] A.E. Eriksson, P.M. Kylsten, T.A. Jones, A. Liljas, Crystallographic studies of inhibitor binding sites in human carbonic anhydrase II: a pentacoordinated binding of the SCN− ion to the zinc at high pH, proteins: structure, Function, and Bioinformatics. 4 (1988) 283–293, https://doi.org/10.1002/PROT.340040407.
[57] Shenghua Huang, Björn Sjöblom, A. Elisabeth Sauer-Eriksson, Bengt-Harald Jonsson, Organization of an efficient carbonic anhydrase: implications for the mechanism based on structure−function studies of a T199P/C206S mutant, Biochemistry. 41 (2002) 7628–7635, https://doi.org/10.1021/BI020053O.
[58] P.-O. Freskgaard, L.-G. Maartensson, P. Jonasson, B.-H. Jonsson, U. Carlsson, Assignment of the contribution of the tryptophan residues to the circular dichroism Spectrum of human carbonic anhydrase II, Biochemistry. 33 (1994) 14281–14288, https://doi.org/10.1021/bi00251a041.
[59] J. Blake-Hall, O. Walker, D. Fushman, Characterization of the overall rotational diffusion of a protein from ¹⁵N relaxation measurements and hydrodynamic calculations, in: Protein NMR Techniques, Humana Press, New Jersey, 2004, pp. 139–160, https://doi.org/10.1385/1-59259-809-9:139.
[60] J. Garíca de la Torre, M.L. Huertas, B. Carrasco, HYDRONMR: prediction of NMR relaxation of globular proteins from atomic-level structures and hydrodynamic calculations, J. Magn. Reson. 147 (2000) 138–146, https://doi.org/10.1006/jmre.2000.2170.
[61] S. Lindskog, P.O. Nyman, Metal-binding properties of human erythrocyte carbonic anhydrases, Biochim. Biophys. Acta (BBA) - Special. Sect. Enzymol. Subj. 85 (1964) 462–474, https://doi.org/10.1016/0926-6569(64)90310-4.
[62] S. Lindskog, A. Ehrenberg, Magnetic susceptibility and near infrared spectra of bovine cobalt carbonic anhydrase, J. Mol. Biol. 24 (1967) 133–137, https://doi.org/10.1016/0022-2836(67)90098-8.